



Mesoporous activated carbon materials with ultrahigh mesopore volume and effective specific surface area for high performance supercapacitors



Yanhong Lu^{a,*}, Suling Zhang^a, Jiameng Yin^a, Congcong Bai^a, Junhao Zhang^a, Yingxue Li^a, Yang Yang^b, Zhen Ge^b, Miao Zhang^b, Lei Wei^a, Maixia Ma^a, Yanfeng Ma^b, Yongsheng Chen^{b,**}

^a School of Chemistry & Material Science, Langfang Teachers University, Langfang, 065000, China

^b The Centre of Nanoscale Science and Technology and Key Laboratory of Functional Polymer Materials, State Key Laboratory and Institute of Elemento-Organic Chemistry, College of Chemistry, Nankai University, Tianjin, 300071, China

ARTICLE INFO

Article history:

Received 4 June 2017

Received in revised form

6 August 2017

Accepted 21 August 2017

Available online 23 August 2017

ABSTRACT

High specific surface area (SSA), especially effective specific surface area (E-SSA) of the active electrode materials is required for high performance supercapacitors. In this work, such materials (e.g. AC-KOH) were obtained using a scalable industrial method from biomass waste material, with controlling the pore size distribution and mesopores as the major contribution. Thus, an electrode material, with ultrahigh mesopore volume of $1.85 \text{ cm}^3 \text{ g}^{-1}$, E-SSA up to $1771 \text{ m}^2 \text{ g}^{-1}$ for organic electrolyte ion (TEA^+) and taking 55% of the total SSA of $3237 \text{ m}^2 \text{ g}^{-1}$ with an excellent conductivity of 33 S m^{-1} , was obtained. With these outstanding properties, the materials demonstrate excellent double-layer capacitance with remarkable rate performance and good cycling stability. The material delivers capacitance up to 222, 202 and 188 F g^{-1} at current density of 1 A g^{-1} in aqueous, organic and ionic liquid electrolyte system, respectively. Meanwhile, it exhibits a high energy density of 80 W h kg^{-1} in ionic liquid electrolyte at a power density of 870 W kg^{-1} . Furthermore, these materials can be produced in large scale from various biomass materials, and thus could be an excellent choice of the high performance materials required in the increasing important supercapacitor industry.

© 2017 Published by Elsevier Ltd.

1. Introduction

Supercapacitors (SCs), also named electrochemical capacitors or ultracapacitors, are attracting intense scientific attention as they can bridge the energy-power gap between the commercial batteries and traditional capacitors [1–3]. Due to their high power density and excellent cycle life, SCs power a wide variety of devices, ranging from small and low-power electronics up to the large energy units applied in such as electric vehicles [4,5]. Activated carbons (ACs) with high specific surface area (SSA), optimal pore size distribution (PSD) and high conductivity are highly desired as

advanced electrode materials for electrochemical double-layer capacitors (EDLCs) [6–10]. EDLCs store charge when electrolyte ions form electric double layers at the surface of oppositely charged electrodes under an externally applied voltage, with the amount of charge stored being proportional to the available SSA of electrode materials [4]. Note that this available SSA is actually the effective SSA (E-SSA) [11,12], which is often mixed up with the total SSA obtained directly from the Brunauer-Emmett-Teller (BET) analysis. E-SSA, the accessible portion of the total SSA for electrolyte ions, is determined by both the total SSA, PSD of the electrode materials and the electrolyte ion size. So it is critical to design an electrode material by controlling both the SSA and PSD for better capacitance performance. Previously, various approaches have been made to increase the total SSA [13–16], but much less has been done to design and achieve the more meaningful high E-SSA by controlling the microstructures of the materials. Though some approaches, such as carbide-derived and template approaches, have been

* Corresponding author. School of Chemistry & Material Science, Langfang Teachers University, Langfang, 065000, China.

** Corresponding author.

E-mail addresses: luyanhong_2003@126.com (Y. Lu), yschen99@nankai.edu.cn (Y. Chen).

reported [17–20] and offered some sort of controlling of the pore structures, most of these materials suffer from either complicated synthesis process of high-cost, and/or the use of toxic chemicals/gases, thus hindering their possible scalable production and wide application in industry. Also, previously a linear relationship between the E-SSA of the electrode materials and their capacitance of devices has been found based on a general model [11,21]. So it would be ideal to design the electrode materials with high E-SSA, not merely high SSA, by controlling the PSDs of materials for high performance SCs.

In this work, such materials, mesoporous activated carbons (AC-KOH) with ultrahigh E-SSA and thus high capacitance performance have been obtained using a simple industrial hydrothermal carbonization and activation approach from the biomass corn straw. The high synergy of total BET SSA of 3237 m² g⁻¹ and an ultrahigh E-SSA reaching up to 1771 m² g⁻¹, together with a good conductivity of 33 S m⁻¹ was achieved by controlling the PSDs and having the mesopore volume of 1.85 cm³ g⁻¹ as the major contribution to the total pore volume. Note, different from most of previously reported carbon materials, the pore structure of our materials could be controlled and optimized with the more important mesopores as the dominated contribution to the overall pore structure. This mesopore dominated structure, leading to a high E-SSA percentage in the total SSA, makes these materials show both high capacitance and rate performance. The capacitor based on this electrode material delivers a high specific capacitance (C_p) of 222 F g⁻¹ in aqueous (6 M KOH), 202 F g⁻¹ in organic (1.0 M TEABF₄/AN) and 188 F g⁻¹ in ion liquid electrolyte (EMIMBF₄) at current density of 1 A g⁻¹, much better than that of commercial activated carbon YP50, and also among the highest of the materials prepared from other carbon sources (details in Data in Brief article). Furthermore, in ionic liquid electrolyte system, the AC-KOH materials exhibit energy density of 80 W h kg⁻¹, also significantly higher than that of YP50 (51 W h kg⁻¹). The outstanding electrochemical performance of these materials can be attributed to their better controlled and optimal microstructures, which not only provides a high E-SSA accessible to the electrolyte ions but also offers abundant mesopore channels for faster ion transportation. Thus, the combined properties in terms of high E-SSA, abundant mesoporous structure, good conductivity and low-cost make these materials a viable choice for the truly industry applications much required for the increasing green energy platform.

2. Experimental

2.1. Materials synthesis

All chemicals used in this study are analytical grade and used directly without further treatment unless otherwise indicated. Distilled water was used in all experiments. The commercially landmark available AC, YP50 was obtained from Tianjin Plannano Energy Technologies Co., Ltd with BET SSA of 1493 m² g⁻¹. The biomass material, air-dry corn straw was collected from local place, and was shattered and sieved through 100 mesh sieve. The collected powders under 150 μm were dried at 120 °C for 24 h under vacuum. The corn straw derived ACs were synthesized through a hydrothermal carbonization and followed by an activation step following our previous procedures [12,22]. Typically, corn straw powders (8.00 g) were added into distilled water (60 mL) and stirred for 2 h. The as-prepared suspension was then transferred to a sealed 100 mL Teflon-lined autoclave, heated to 180 °C and maintained at this temperature for 12 h. After the autoclave was cooled to room temperature, the hydrothermal product was filtered, washed with distilled water and finally dried in vacuum at 120 °C for 24 h. For the optimal process, the hydrothermal product

was mixed with different activation agents at the weight ratio of 1–4, placed into a nickel boat in a horizontal tube furnace and heated to 900 °C for 1 h at 5 °C min⁻¹ under Ar. After cooling to room temperature, the products were thoroughly washed with 0.1 M HCl and distilled water until the pH value reached 7. Finally, the collected sample was dried in a vacuum oven at 120 °C for 12 h. KOH, ZnCl₂, K₂CO₃ and Na₂CO₃ were used as the activation agents, and the corresponding final products were labeled as AC-KOH, AC-ZnCl₂, AC-K₂CO₃ and AC-Na₂CO₃, respectively. Note other ratios other than 4:1 such as 2:1 and 5:1 with activation agents have been tested for the activation step, including the case of KOH, where the corresponding products are named as AC-KOH-2:1 and AC-KOH-5:1, respectively. The activation production yield (η) was calculated with the weight ratio of the activation product to the hydrothermal product.

2.2. Characterization

X-ray diffraction (XRD) was carried out using a Rigaku D/Max-2500 diffractometer with Cu K_α radiation. The interlayer spacing (d_{002}) was calculated from the Bragg peaks using the Bragg law: $n\lambda = 2d\sin\theta$, where λ is the wave length of the X-ray radiation and θ is the Bragg angle. The height (L_c) of stacking carbon domains was calculated from (002) peak using Scherrer's equation: $L_c = K\lambda/(\beta_c \times \cos\theta)$, where K is the shape factor (0.89), λ is the wave length of the X-ray radiation, β_c is the full widths at half maximum (FWHM) of the diffraction peaks and θ is the Bragg angle. Raman spectra were examined with a LabRAM HR Raman spectrometer using laser excitation at 514.5 nm. Lorentzian fitting was carried out to confirm the positions and FWHM of the D and G bands. The size (L_a) of carbon domains can be carried out by L_a (nm) = $(560/E^4)(I_D/I_G)^{-1}$, where E is the laser energy (2.41 eV), I_D and I_G are the intensities of the D and G bands, respectively. X-ray photoelectron spectroscopy (XPS) analysis was obtained using AXIS HIS 165 spectrometer (Kratos Analytical) with a monochromatized Al K_α X-ray source (1486.71 eV photons). The nitrogen adsorption/desorption analysis was done at 77 K on a Micromeritics ASAP 2020 apparatus. The BET method was employed for the SSA, and the density functional theory (DFT) method was used for the PSD analysis. Scanning electron microscopy (SEM) images were obtained on a Phenom Pro SEM. High resolution transmission electron microscopy (HR-TEM) was conducted in a FEI Tecnai G2 F20 electron microscope using an acceleration voltage of 200 kV.

2.3. Fabrication of supercapacitors

The supercapacitor test cells were fabricated by a symmetrical two-electrode system [23,24]. The electrode materials, mixed with carbon black (Super P, Timcal) and polytetrafluoroethylene (PTFE, solid powder, Dupont) at the weight ratio of 85:5:10, was rolled into 80–100 μm thickness sheets and punched into 12 mm diameter electrodes. After dried at 120 °C for 6 h under vacuum, the electrodes were weighted and hot pressed onto Al foils with conducting carbon coating (or foam Ni) and then dried at 180 °C for 6 h under high vacuum. The dry electrodes were transferred into a glove box filled with Ar to assemble the coin-type supercapacitors which consisted of two current collectors, electrolyte, two electrodes with identical weight and a separator sandwiched. 6 M KOH, 1.0 M TEABF₄/AN and EMIMBF₄ electrolytes were investigated respectively.

2.4. Electrochemical measurements

All the electrochemical tests were performed at room temperature. Cyclic voltammetry (CV) measurements were carried out using

a CHI660C electrochemical analyzer (Shanghai Chenhua Instruments Co., Ltd.). Galvanostatic charge-discharge cycle tests were performed using a battery test system (LAND CT2001A model, Wuhan LAND Electronics, Ltd.). The applied voltage windows was 0–1.0 V for KOH, 0–2.7 V for TEABF₄/AN and 0–3.5 V for EMIMBF₄ electrolyte respectively. The electrochemical impedance spectroscopy (EIS) measurements were carried out in the range of 100 kHz to 10 mHz on a P4000 electrochemical workstation (Princeton, USA). The specific capacitance C_p (F g⁻¹) was calculated according to:

$$C_p = \frac{4I}{m dV/dt}$$

where I (A) is the constant current, m (g) is the total mass of the active materials on the two single electrodes and dV/dt (V s⁻¹) is the slope obtained by fitting a straight line to the discharge curve over the range from V (the voltage at the beginning of discharge) to $V/2$. The energy density, E_{cell} (W h kg⁻¹), was calculated using the formula $E_{\text{cell}} = C_p V^2/8$, where C_p (F g⁻¹) is the specific capacitance of the device and V (V) is the voltage. The power density, P (W kg⁻¹), was calculated according to the formula $P = E/\Delta t$, where E (W h kg⁻¹) is the energy density of the device and Δt (s) is the discharge time.

The electronic conductivities of AC-KOH and YP50 were measured using the previous reported method [12,24]. Typically, the sample was mixed with 2 wt% PTFE as a binder, and homogenized in an agate mortar. Then it was rolled into 10–20 μm thickness sheets and cut into 1 × 3 cm² and pressed at 10 MPa for 10 s. Then it was covered with the copper foil on both sides and measured using a multimeter. The conductivity of the film was calculated using the formula $\lambda = L/R_x \cdot W \cdot d$, where λ is the conductivity of the sample, L , W , d is the length, width and thickness of the sheet respectively, and R_x is the resistance of the sheet tested by the multimeter.

2.5. Calculation of the E-SSA and theoretical specific capacitance

The E-SSA and theoretical specific capacitance of the electrode material were calculated following our early works [11,12]. As a typical example, the E-SSA was obtained according to the cumulative DFT SSA, the PSD of the carbon materials and the electrolyte ion size (details in Data in Brief article). The data of DFT SSA and PSD were obtained from the BET analysis directly. For the electrolyte ion size used for the calculation, both the cases of solvent free (bare) and solvated ions should be considered. For the case of TEABF₄ in AN, the diameters of solvent free (bare) and solvated TEA⁺ cation are 0.684 and 1.32 nm, respectively, which is larger than that of BF₄⁻ anion (0.458 nm), so the sizes of TEA⁺ cations were used for the E-SSA calculation [11,12]. When the pore width of the carbon material is larger than 0.684 nm (the bare size of TEA⁺ cation) but smaller than 1.32 nm (the size of solvated TEA⁺ cation), the bare TEA⁺ ion size was used for the calculation. While when the pore width of the carbon material is larger than 1.32 nm, the solvated TEA⁺ ions was then used. Both parts were then added up as the total E-SSA. With the E-SSA, the theoretical capacitance of the carbon materials in TEABF₄/AN electrolyte was calculated based on the effective ionic diameter model discussed in our early work [12].

3. Results and discussion

3.1. Structure and morphology characterization

As discussed above, to achieve excellent performance SCs, it is critical to achieve high E-SSA, rather than just high total SSA. This

requires to control both the morphology of the starting carbon sources and the activation process for an optimal product pore structure [11]. So, based on the morphology analysis, a cheap agriculture waste of corn straw was selected as the carbon source and an industrial hydrothermal carbonization and chemical activation process was applied. The SEM image of the carbon source corn straw (Fig. 1a) shows a well-organized honeycomb porous structure. If the treatment and/or activation process were controlled properly, a mesoporous structure could be achieved, thus to offer a high E-SSA. As shown in Fig. 1b, after hydrothermal treatment, the layered and porous structure were kept for the carbonized product. This unique porous/layered structure of the hydrothermal products makes them much easier to undergo the further activation process of some micropores, leading to abundant mesopores and high E-SSA. As will be presented below, various activation agents and with different ratios were tested, and Fig. 1c exhibits the loose carbon structures of the best product AC-KOH after activation process with KOH. The HR-TEM image in Fig. 1d shows some clear porous structure on the surface of AC-KOH, formed by the evaporation of activation agent. This would generate abundant void space during activation after the subsequent removal of untreated activation agent via washing with deionized water [25]. In addition to the high E-SSA, this plenty of mesopores also provide favorable and more efficient paths for transportation of electrolyte ions, desired for a high rate performance.

XPS analysis was performed to study the surface chemical composition and atomic percentage of the surface elements. In Fig. 2a, clear peaks of C1s (285 eV) and O1s (532 eV) were observed. The contents of C and O elements in AC-KOH are estimated as 94.46% and 4.87%, respectively, similar to that of commercial YP50 (details in Data in Brief article). The high resolution C1s spectra of AC-KOH (Fig. 2b) can be deconvoluted into three individual component peaks, corresponding to C=C (284.6 eV), C–O (285.5 eV) and O–C=O (288.2 eV), respectively [21,24]. The overwhelming strong peak of C=C at 284.6 eV demonstrates that most of the carbon atoms are sp² carbons. The relatively weak peak of C–O at 285.5 eV indicates the existence of small amount of the surface oxygen-containing groups, which can contribute to the hydrophilicity and wettability of material surface and facilitate the accessibility of the electrolyte ions.

Fig. 2c show the N₂ adsorption/desorption isotherms of the prepared series of ACs using different activation agents and the compared YP50. All the samples display the typical characteristics of type-IV isotherms with hysteresis loop, indicating a combination of microporous/mesoporous structure [25]. The optimal AC-KOH exhibits much more significant hysteresis than that of AC-K₂CO₃, AC-Na₂CO₃, AC-ZnCl₂ and the industry landmark material YP50 in the relative pressure (P/P_0) range of 0.4–0.9, showing much higher amount of mesopores in AC-KOH than other ACs using the same starting materials and under the same procedure. The calculated structure parameters of series of carbon materials, including BET SSA, total, micro-/meso-pore volume, E-SSA for organic electrolyte ion of TEA⁺ and the production yields are summarized in Table 1 (details in Data in Brief article). As can be seen, AC-KOH material gives the highest E-SSA of 1771 m² g⁻¹ with 55% contribution to the total SSA of 3237 m² g⁻¹, and a mesopore volume of 1.85 cm³ g⁻¹ with 81.5% proportion of the total pore volume of 2.27 cm³ g⁻¹, which all are superior than the other ACs using different activation agents and the commercial YP50. These results indicate that activation agents have strong impact for the SSA and pore size distribution of products, and thus changing the product's E-SSAs significantly. Fig. 2d show the PSDs of the best AC-KOH material and the compared YP50. It is clearly illustrated that the pore structure of AC-KOH material is mainly in the range of mesopore with

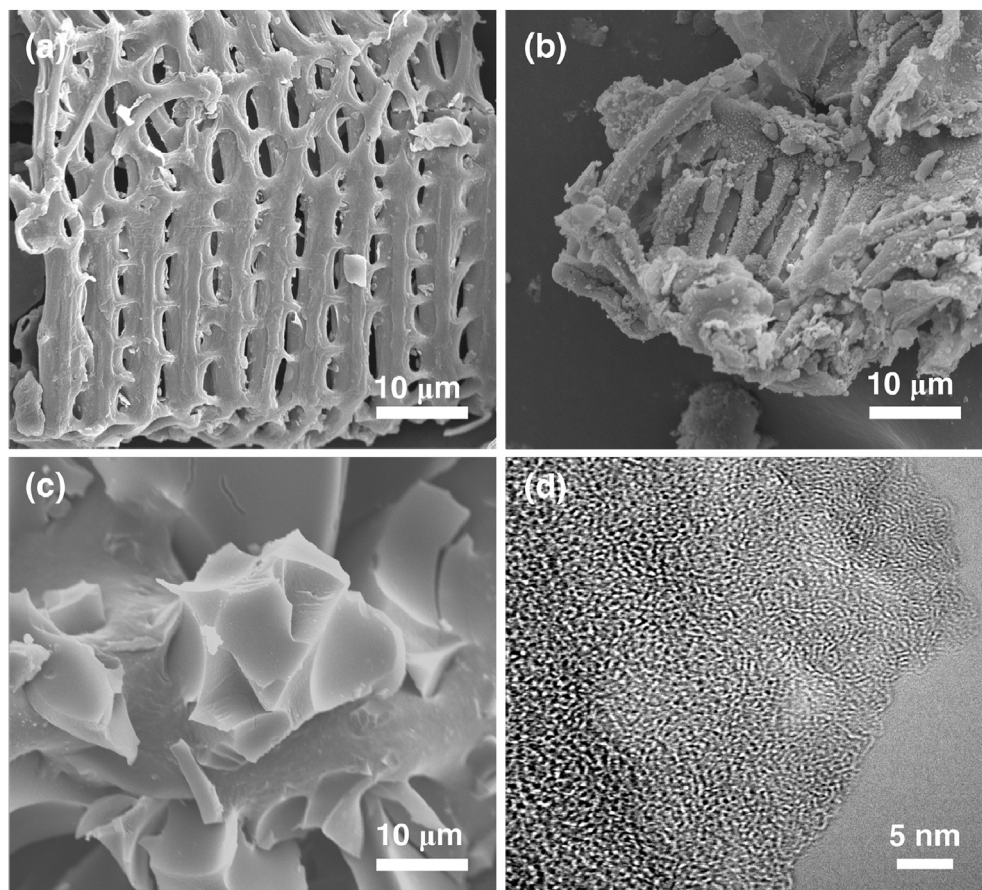


Fig. 1. The SEM images of (a) carbon source of corn straw, (b) hydrothermal product of corn straw, (c) activation product AC-KOH and (d) HR-TEM of AC-KOH.

adsorption average pore width (W_p) of 3.23 nm, much different from other materials. From Table 1 and Fig. 1 in the corresponding Data in Brief article, the pore width of AC-ZnCl₂, AC-Na₂CO₃, AC-KOH-2:1 and AC-KOH-5:1 are 3.07, 2.27, 2.14 and 2.58 nm, respectively, all lower than that of AC-KOH (3.23 nm). Especially, AC-K₂CO₃ and YP50 are mainly consisting of the micropores and the average pore sizes are only 1.86 and 1.98 nm, respectively. Fig. 2e show the distribution of cumulative pore volume with the pore size of AC-KOH, indicating that the proportion of the mesopore volume reaches up to 81.5%, dramatically higher than that of other prepared ACs and YP50 (Table 1).

For the best AC-KOH material, its morphology and high SSA were further analyzed using XRD and Raman spectra. As shown in Fig. 2f, the two weak and broad diffraction peaks at $\sim 25^\circ$ and 42° in the XRD patterns of AC-KOH correspond to the (002) and (100) planes, indicative of its much lower ordering. The inter layer spacing (d_{002}) of AC-KOH, calculated from the center position of (002) peak, is about 0.416 nm, significantly larger than that of graphite (0.335 nm), implying a random combination of graphitic and turbostratic stacking [25,26]. The thickness of the carbon domains in AC-KOH was estimated from the XRD lattice parameters and the average domain's height (L_c) can be approximately determined to be 0.79 nm by using the Scherrer's equation, which is close to that of the earlier reported sp² carbon materials with high SSA [21,27]. The characteristic of highly disordered carbons and the size is also supported by the results from Raman studies. In Fig. 2g, the D band at 1350 cm⁻¹ for disordered carbon crystallites, together with the G band at 1586 cm⁻¹ (attributed to crystalline graphite), was observed. The large value of the full width at half maximum of

D and G bands (~ 272 and 109, respectively) and the high value of the ratio of integrated intensities of D and G bands ($I_D/I_G = 2.5$) demonstrate a high degree of structural disorder for porous carbons [28]. The estimated average in-plane size (L_a) of the carbon domains in AC-KOH was ~ 6.65 nm based on Raman analysis [27]. This small carbon domain size, indicating a significant contribution of the edge part to the SSA, thus would lead to a high SSA as reported earlier [11,27]. Using these morphology data, the theoretical SSA was estimated to be 3200–3500 m² g⁻¹ [27], consistent with the experimental SSA.

The electronic conductivity of AC-KOH was measured to be 33 S m⁻¹, much higher than that of YP50 (9 S m⁻¹). Since the state of the art ACs used in commercial has significantly lower conductivity and requires significant amount of addition of conducting materials, its inherent higher electronic conductivity should make this material to have a better rate performance with similar formula of the electrode composition.

3.2. Electrochemical performance

The AC-KOH sample exhibits dominantly mesoporous structure and high E-SSA compared with other prepared ACs. Thus, it was further studied for EDLC application. The theoretical capacitance of AC-KOH electrode material in TEABF₄/AN electrolyte at current density of 1 A g⁻¹ was estimated at 204 F g⁻¹ based on the previous reported model using its E-SSA [12]. The details for the calculation of such theoretical capacitance was presented in the Experimental section. Its practical electrochemical performance was then evaluated following the widely accepted standard

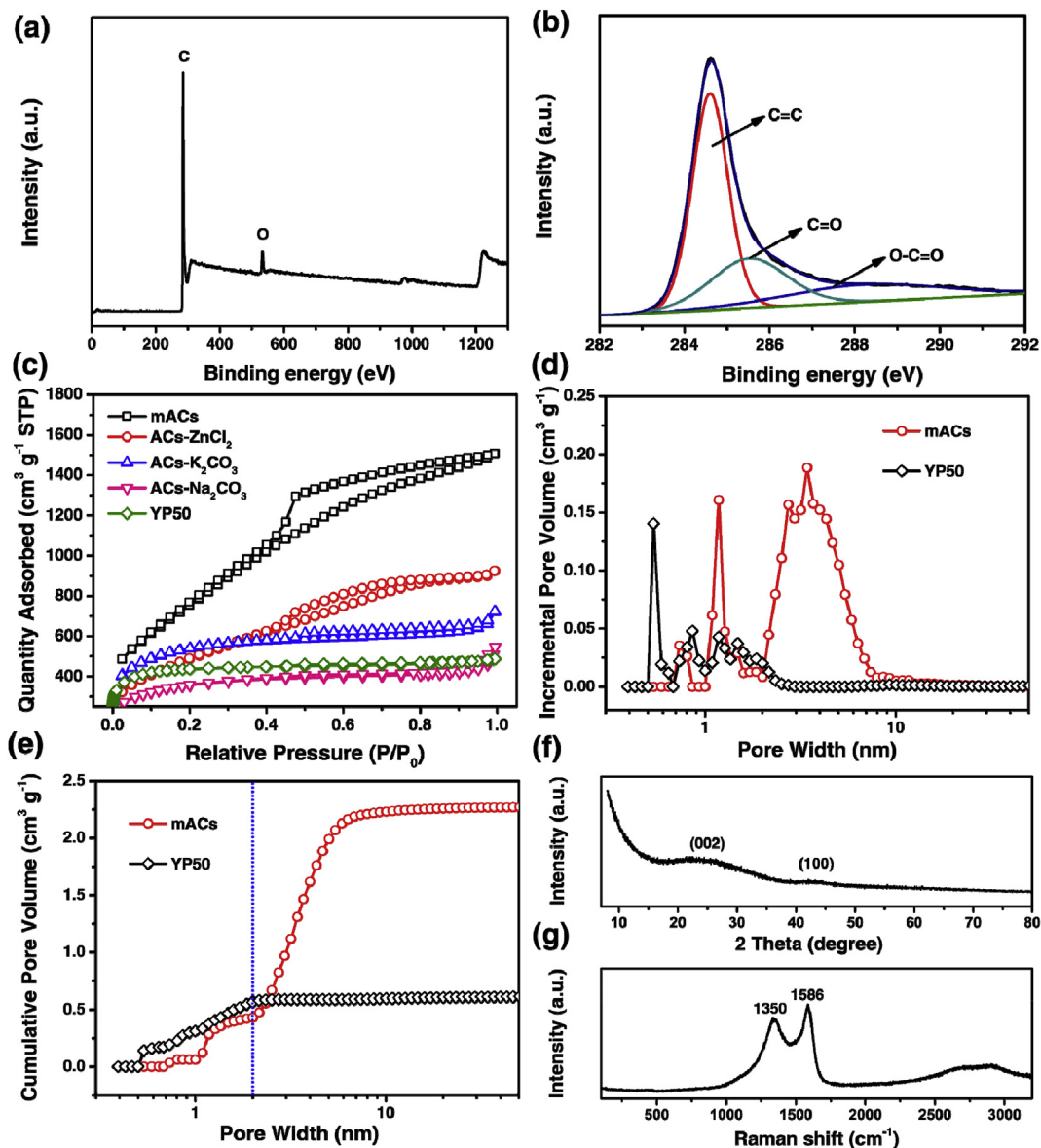


Fig. 2. Structure analysis of prepared ACs and the compared commercial YP50. (a) XPS survey spectrum. (b) High resolution C1s spectra. (c) Adsorption/desorption isotherms of ACs activated using different activation agents and YP50. (d) PSDs of AC-KOH and YP50 based on the DFT method from the nitrogen adsorption data. (e) The distribution of cumulative pore volume with pore width for AC-KOH and YP50. The inset vertical dashed line demonstrated the boundary of micropore and mesopore. (f) XRD and (g) Raman results of AC-KOH. (A colour version of this figure can be viewed online.)

Table 1

The SSA, porosity parameters and the production yields of prepared ACs and the control commercial YP50.

Sample	$S_{\text{BET}}^{\text{a}}$ ($\text{m}^2 \text{g}^{-1}$)	$V_{\text{tot}}^{\text{b}}$ ($\text{cm}^3 \text{g}^{-1}$)	$V_{\text{mic}}^{\text{c}}$ ($\text{cm}^3 \text{g}^{-1}$)	$V_{\text{mes}}^{\text{d}}$ ($\text{cm}^3 \text{g}^{-1}$)	$V_{\text{mes}}/V_{\text{tot}}^{\text{e}}$ (%)	E-SSA ($\text{m}^2 \text{g}^{-1}$)	W_{p}^{f} (nm)	η^{g} (%)
AC-KOH	3237	2.27	0.42	1.85	81.5	1771	3.23	7.20
AC-ZnCl ₂	1631	1.04	0.25	0.79	76.0	833	3.07	41.0
AC-K ₂ CO ₃	1622	0.89	0.47	0.42	47.2	892	1.86	21.2
AC-Na ₂ CO ₃	1254	0.63	0.35	0.28	46.0	510	2.27	21.1
AC-KOH-2:1	2346	1.08	0.54	0.54	50.0	1065	2.14	9.78
AC-KOH-5:1	2264	1.23	0.35	0.88	71.5	1183	2.58	2.46
YP50	1493	0.62	0.54	0.08	12.9	713	1.98	–

^a BET total specific surface area.

^b Total pore volume.

^c Micro pore volume.

^d Meso pore volume.

^e The ratio of mesopore volume to total pore volume.

^f The adsorption average pore width.

^g The activation production yields.

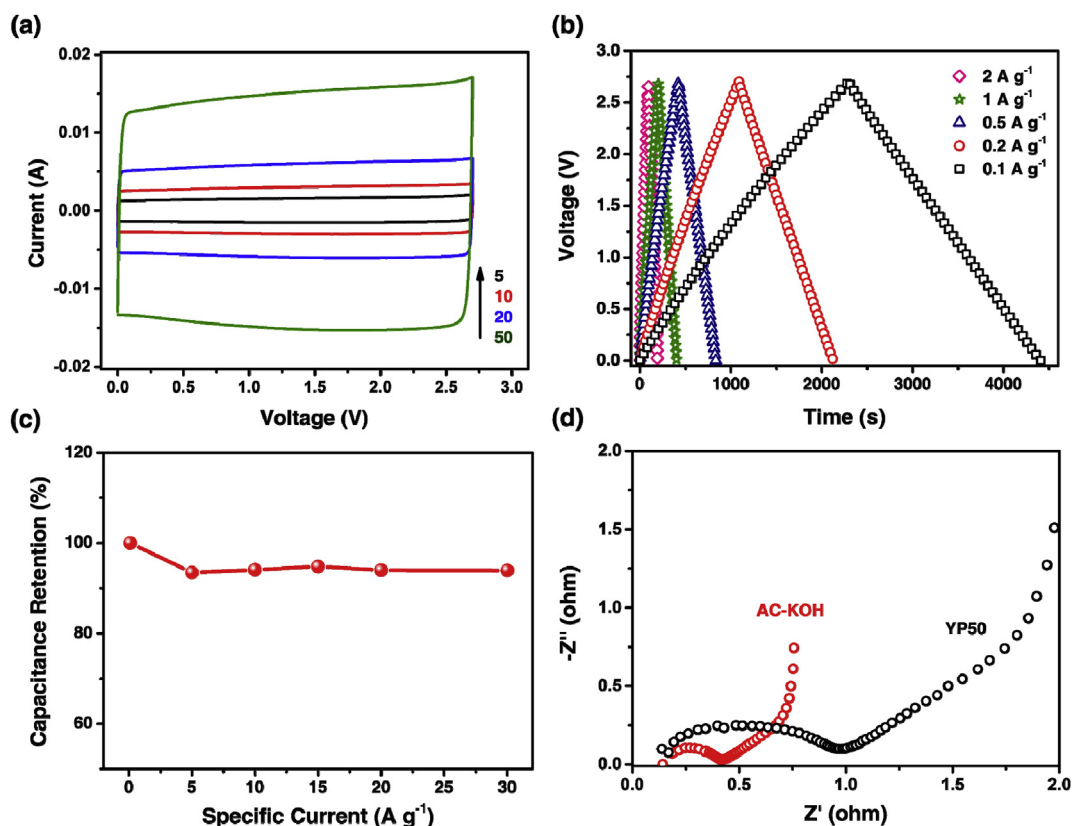


Fig. 3. Electrochemical performance of AC-KOH and YP50 based SCs in TEABF₄/AN electrolyte system. (a) CV curves of AC-KOH based SC measured at the scan rates of 5, 10, 20 and 50 mV s⁻¹ in the potential range of 0–2.7 V. (b) Galvanostatic charge/discharge curves for AC-KOH based SC tested at current densities from 0.1 to 2 A g⁻¹. (c) Rate performance for AC-KOH based supercapacitor tested at current densities from 0.1 to 30 A g⁻¹. (d) Nyquist plots of AC-KOH and YP50 based SCs. (A colour version of this figure can be viewed online.)

method using two-electrode testing cells with KOH, TEABF₄/AN and EMIMBF₄ as the electrolytes, respectively [21,29]. Fig. 3 illustrates the electrochemical performance of AC-KOH and YP50 based SCs in TEABF₄/AN electrolyte system. The CVs of AC-KOH (Fig. 3a) in the voltage range of 0–2.7 V at the scan rates of 5, 10, 20 and 50 mV s⁻¹ all display nearly perfect rectangular shape without any redox peak. This demonstrates the ideal behavior of EDLC with fast charge/discharge processes [23]. The galvanostatic charge/discharge curves of AC-KOH at different current densities are close

to an isosceles triangle shape (Fig. 3b). Especially, at a low current density of 0.1 A g⁻¹, the charging curves are also generally highly symmetric, similar as their corresponding discharging counterparts, revealing high capacitive reversibility and the ideal EDLC characteristics, consistent with the CV results above. The capacitance of AC-KOH based supercapacitor is 202 F g⁻¹ at a current density of 1 A g⁻¹ (Fig. 2 in Data in Brief article), consistent with the calculated theoretical C_p value (204 F g⁻¹), which is significantly superior than that of the control sample of YP50 (100 F g⁻¹) and

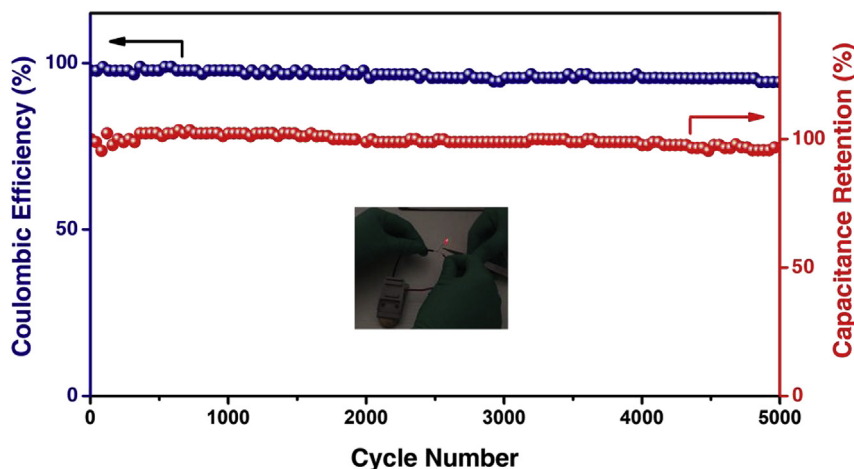


Fig. 4. Cycling stability for AC-KOH based supercapacitor after 5000 cycles, measured at a current density of 2 A g⁻¹ within the potential range from 0 to 2.7 V. The inset is the lightened LED light. (A colour version of this figure can be viewed online.)

other reported biomass derived AC electrode materials [30,31]. Generally, the capacitance of AC materials would decrease significantly at higher current density, particularly for the cases where micropore is dominated. But in our case, it was found that the capacitance retains very well when the current density increased. As shown in Fig. 3c and Fig. 3 in the corresponding Data in Brief article, the specific capacitance of the AC-KOH electrode material retained at ~94% even when the current density increased from 0.1 to 30 A g⁻¹, indicating an excellent rate capability. The high retention of capacitance at high current density should be attributed to the suitable mesoporous structures of AC-KOH, whose optimal pore structure can provide smooth and convenient ion transfer pathways for quick transportation of electrolyte ions and rapid formation the electric double layers.

The charge transfer resistance and ion diffusion performance were evaluated by the EIS measurements at a frequency range of 100 kHz to 10 mHz. Fig. 3d shows the Nyquist plots for AC-KOH and YP50 based SCs. In the low-frequency region, both AC-KOH and YP50 plots exhibit an oblique line, indicating a diffusion controlled electrode process. The relatively steeper slope of AC-KOH plot suggests that the electric double layers in AC-KOH based device is easier to establish than that of YP50. The Warburg resistance at the 45° portion of AC-KOH is shorter than that of YP50, indicating a shorter ion diffusion path for AC-KOH [24]. In the high-frequency region, the AC-KOH based supercapacitor exhibits a smaller equivalent series resistance (0.42 Ω) than that of YP50 (0.97 Ω), indicating a lower charge transfer resistance, which is a result of the excellent conductivity of AC-KOH. All these are consistent with its mesopore dominated structure.

The cycling stability of AC-KOH electrode materials in TEABF₄/AN was also performed using the galvanostatic charge/discharge method at a current density of 2 A g⁻¹, as shown in Fig. 4. After 5000 cycles, the capacitance is kept ~96%, indicating an excellent life time.

Similarly, AC-KOH was evaluated using the aqueous and ionic liquid electrolyte systems, and also demonstrated excellent performance. For example, in 6 M KOH electrolyte (Fig. 4 in Data in Brief article), it gives as such as high capacitance of 260 and 222 F g⁻¹ at current density of 0.1 and 1 A g⁻¹, respectively, superior than that of the YP50 and previous works [32–34]. In ionic liquid, its capacitance and energy density reached 188 F g⁻¹ at current density of 1 A g⁻¹ and 80 W h kg⁻¹ at power density of 870 W kg⁻¹, respectively, much higher than that of YP50 (120 F g⁻¹, 51 W h kg⁻¹ at power density of 870 W kg⁻¹) (Fig. 5 in Data in Brief article) under the same test condition and the reported works [31,35–37]. With this high energy density, the device was assembled for lighting up a light emitting diode (LED) light. As shown in the inset of Fig. 4 (Fig. 6 and supplementary video in Data in Brief article), a red LED with a working potential around 2.2 V and working power about 40 mW could be lighted up for ~30 min when it was connected to the fully charged coin-type supercapacitor.

4. Conclusion

With appropriate structure of the starting carbon source and activation approach, a carbon material with optimal mesopore dominated morphology and high E-SSA was obtained using an industrial scalable method. Due to its high E-SSA of 1771 m² g⁻¹ for organic electrolyte ion of TEA⁺, mesopore volume of 1.85 cm³ g⁻¹, average pore width of 3.23 nm and excellent electronic conductivity of 33 S m⁻¹, the electrode materials offer 222, 202 and 188 F g⁻¹ at current density of 1 A g⁻¹ in aqueous, organic and ionic liquid electrolyte systems, respectively, and exhibit high energy density of 80 W h kg⁻¹ in ionic liquid. Thus, this low cost and high performance material may offer a competent choice as the active

material of EDLCs in industry.

Acknowledgements

The authors gratefully acknowledge the financial support from the National Natural Science Foundation of China (NSFC, 51502125), the Natural Science Foundation of Hebei Province of China (Grant E2016408035, B2017408042) and the Research Project of Hebei Education Department of China (BJ2016044).

References

- [1] M. Winter, R.J. Brodd, What are batteries, fuel cells, and supercapacitors? *Chem. Rev.* 104 (10) (2004) 4245–4270.
- [2] G. Wang, L. Zhang, J. Zhang, A review of electrode materials for electrochemical supercapacitors, *Chem. Soc. Rev.* 41 (2) (2012) 797–828.
- [3] K. Xie, X. Qin, X. Wang, Y. Wang, H. Tao, Q. Wu, et al., Carbon nanocages as supercapacitor electrode materials, *Adv. Mater.* 24 (3) (2012) 347–352.
- [4] A. Vlad, A. Balducci, Supercapacitors: porous materials get energized, *Nat. Mater.* 16 (2) (2017) 161–162.
- [5] L.L. Zhang, R. Zhou, X.S. Zhao, Graphene-based materials as supercapacitor electrodes, *J. Mater. Chem.* 20 (29) (2010) 5983–5992.
- [6] C. Lei, N. Amini, F. Markoulidis, P. Wilson, S. Tennison, C. Lekakou, Activated carbon from phenolic resin with controlled mesoporosity for an electric double-layer capacitor (EDLC), *J. Mater. Chem. A* 1 (19) (2013) 6037–6042.
- [7] H. Jiang, P.S. Lee, C. Li, 3D carbon based nanostructures for advanced supercapacitors, *Energy Environ. Sci.* 6 (1) (2013) 41–53.
- [8] L.L. Zhang, X.S. Zhao, Carbon-based materials as supercapacitor electrodes, *Chem. Soc. Rev.* 38 (9) (2009) 2520–2531.
- [9] Q. Wu, L. Yang, X. Wang, Z. Hu, From carbon-based nanotubes to nanocages for advanced energy conversion and storage, *Acc. Chem. Res.* 50 (2) (2017) 435–444.
- [10] J. Zhang, M. Terrones, C.R. Park, R. Mukherjee, M. Monthieux, N. Koratkar, et al., Carbon science in 2016: status, challenges and perspectives, *Carbon* 98 (2016) 708–732.
- [11] L. Zhang, X. Yang, F. Zhang, G. Long, T. Zhang, K. Leng, et al., Controlling the effective surface area and pore size distribution of sp² carbon materials and their impact on the capacitance performance of these materials, *J. Am. Chem. Soc.* 135 (15) (2013) 5921–5929.
- [12] Y. Lu, G. Long, L. Zhang, T. Zhang, M. Zhang, F. Zhang, et al., What are the practical limits for the specific surface area and capacitance of bulk sp² carbon materials? *Sci. China Chem.* (2015) 1–7.
- [13] B. Li, F. Dai, Q. Xiao, L. Yang, J. Shen, C. Zhang, et al., Activated carbon from biomass transfer for high-energy density lithium-ion supercapacitors, *Adv. Energy Mater.* 6 (18) (2016).
- [14] M.S. Balathanigaimani, W.-G. Shim, M.-J. Lee, C. Kim, J.-W. Lee, H. Moon, Highly porous electrodes from novel corn grains-based activated carbons for electrical double layer capacitors, *Electrochem Commun.* 10 (6) (2008) 868–871.
- [15] D. Wang, Z. Geng, B. Li, C. Zhang, High performance electrode materials for electric double-layer capacitors based on biomass-derived activated carbons, *Electrochim. Acta* 173 (2015) 377–384.
- [16] J. Wang, M. Chen, C. Wang, J. Wang, J. Zheng, Preparation of mesoporous carbons from amphiphilic carbonaceous material for high-performance electric double-layer capacitors, *J. Power Sources* 196 (1) (2011) 550–558.
- [17] Y. Gogotsi, A. Nikitin, H. Ye, W. Zhou, J.E. Fischer, B. Yi, et al., Nanoporous carbide-derived carbon with tunable pore size, *Nat. Mater.* 2 (9) (2003) 591–594.
- [18] P.-C. Gao, W.-Y. Tsai, B. Daffos, P.-L. Taberna, C.R. Perez, Y. Gogotsi, et al., Graphene-like carbide derived carbon for high-power supercapacitors, *Nano Energy* 12 (2015) 197–206.
- [19] Y. Fang, Y. Lv, R. Che, H. Wu, X. Zhang, D. Gu, et al., Two-dimensional mesoporous carbon nanosheets and their derived graphene nanosheets: synthesis and efficient lithium ion storage, *J. Am. Chem. Soc.* 135 (4) (2013) 1524–1530.
- [20] H. Nishihara, T. Kyotani, Templated nanocarbons for energy storage, *Adv. Mater.* 24 (33) (2012) 4473–4498.
- [21] Y. Lu, Y. Huang, F. Zhang, L. Zhang, X. Yang, T. Zhang, et al., Functionalized graphene oxide based on p-phenylenediamine as spacers and nitrogen dopants for high performance supercapacitors, *Chin. Sci. Bull.* 59 (16) (2014) 1809–1815.
- [22] L. Zhang, F. Zhang, X. Yang, K. Leng, Y. Huang, Y. Chen, High-performance supercapacitor electrode materials prepared from various pollens, *Small* 9 (8) (2013) 1342–1347.
- [23] Y. Wang, Z. Shi, Y. Huang, Y. Ma, C. Wang, M. Chen, et al., Supercapacitor devices based on graphene materials, *J. Phys. Chem. C* 113 (30) (2009) 13103–13107.
- [24] Y. Lu, F. Zhang, T. Zhang, K. Leng, L. Zhang, X. Yang, et al., Synthesis and supercapacitor performance studies of N-doped graphene materials using o-phenylenediamine as the double-N precursor, *Carbon* 63 (0) (2013) 508–516.
- [25] W. Feng, P. He, S. Ding, G. Zhang, M. He, F. Dong, et al., Oxygen-doped activated carbons derived from three kinds of biomass: preparation,

- characterization and performance as electrode materials for supercapacitors, *RSC Adv.* 6 (7) (2016) 5949–5956.
- [26] J. Ding, H. Wang, Z. Li, K. Cui, D. Karpuzov, X. Tan, et al., Peanut shell hybrid sodium ion capacitor with extreme energy-power rivals lithium ion capacitors, *Energy Environ. Sci.* 8 (3) (2015) 941–955.
- [27] L. Zhang, F. Zhang, X. Yang, G. Long, Y. Wu, T. Zhang, et al., Porous 3D graphene-based bulk materials with exceptional high surface area and excellent conductivity for supercapacitors, *Sci. Rep.* (2013) 3.
- [28] L. Wei, M. Sevilla, A.B. Fuertes, R. Mokaya, G. Yushin, Polypyrrole-derived activated carbons for high-performance electrical double-layer capacitors with ionic liquid electrolyte, *Adv. Funct. Mater.* 22 (4) (2012) 827–834.
- [29] M.D. Stoller, S. Park, Y. Zhu, J. An, R.S. Ruoff, Graphene-based ultracapacitors, *Nano Lett.* 8 (10) (2008) 3498–3502.
- [30] D. Bhattacharjya, J.-S. Yu, Activated carbon made from cow dung as electrode material for electrochemical double layer capacitor, *J. Power Sources* 262 (2014) 224–231.
- [31] A.K. Mondal, K. Kretschmer, Y. Zhao, H. Liu, C. Wang, B. Sun, et al., Nitrogen-doped porous carbon nanosheets from eco-friendly eucalyptus leaves as high performance electrode materials for supercapacitors and lithium ion batteries, *Chem. Eur. J.* 23 (15) (2017) 3683–3690.
- [32] L. Zhu, F. Shen, R.L. Smith Jr., L. Yan, L. Li, X. Qi, Black liquor-derived porous carbons from rice straw for high-performance supercapacitors, *Chem. Eng. J.* 316 (2017) 770–777.
- [33] D. Momodu, M. Madito, F. Barzegar, A. Bello, A. Khaleed, O. Olaniyan, et al., Activated carbon derived from tree bark biomass with promising material properties for supercapacitors, *J. Solid State Electrochem.* 21 (3) (2017) 859–872.
- [34] M. Jiang, J. Zhang, L. Xing, J. Zhou, H. Cui, W. Si, et al., KOH-activated porous carbons derived from chestnut shell with superior capacitive performance, *Chin. J. Chem.* 34 (11) (2016) 1093–1102.
- [35] C. Liu, G. Han, Y. Chang, Y. Xiao, M. Li, W. Zhou, et al., Properties of porous carbon derived from cornstalk core in high-performance electrochemical capacitors, *Chemelectrochem* 3 (2) (2016) 323–331.
- [36] Y. Wei, Activated carbon microtubes prepared from plant biomass (poplar catkins) and their application for supercapacitors, *Chem. Lett.* 43 (2) (2014) 216–218.
- [37] A. Sanchez-Sanchez, M.T. Izquierdo, J. Ghanbaja, G. Medjandi, S. Mathieu, A. Celzard, et al., Excellent electrochemical performances of nanocast ordered mesoporous carbons based on tannin-related polyphenols as supercapacitor electrodes, *J. Power Sources* 344 (2017) 15–24.